LA-UR-02-3794

Approved for public release;
distribution is unlimited.

Title: CONSISTENT METRICS FOR CODE VERIFICATION

Author(s) James R. Kamm, CCS-2
William J. Rider, CCS-2
Jerry S. Brock, X-5

Date: June 2002

Photograph by Chris J. Lindberg

Los Alamos
NATIONAL LABORATORY

Consistent Metrics for Code Verification

James R. Kamm, William J. Rider, Jerry S. Brock

Los Alamos National Laboratory
Los Alamos, NM 87545 USA

June 20, 2002

LA-UR-02-3794

Contents

Abstract

In this report we describe a consistent set of metrics for conducting verification analysis. These metrics are based on the procedure known as asymptotic convergence analysis. This process provides the primary metric used in code verification, viz., the asymptotic convergence rate. This value quantifies the convergence properties, relative to an exact or semi-exact solution, of a specific software implementation of a numerical algorithm for solving the discretized forms of continuum equations. Evaluation of this metric provides unambiguous demonstration of the code convergence properties, representing the essence of verification analysis and forming a foundational part of the evidence by which software quality is established. We provide the necessary background to implement convergence analysis on a variety of problems and give examples of this process. This report contains sufficient information to extend the basic approach provided herein to a broad spectrum of applications.

1 Introduction

In this report we provide a brief description of asymptotic convergence analysis, which forms the primary metric by which to demonstrate evidence of code verification. This metric is the fundamental tool used in code verification, as it allows one to quantify the convergence rate of a specific software implementation of a given numerical algorithm. Such software is used to obtain numerical solutions of a set of discretized equations corresponding to the equations that describe some continuous process. The demonstration of code convergence represents the essence of verification analysis and forms a foundational part of the evidence by which software quality is established.

Virtually all of the description provided herein is couched in the framework of analyzing algorithms for the discretization of partial differential equations (PDEs), specifically, the PDEs used in hydrocodes (see [1] for an overview of hydrocodes). The analysis provided herein is applicable to a range of numerical algorithms based on the discretization of continuous models; moreover, these procedures are applicable to computational investigations including calculation verification and the experimental simulation that underpins validation.

The primary nomenclature and procedures are presented in §2, which describes pointwise asymptotic convergence analysis in one dimension. The notions, relations, and approach given in this section are modified in the subsequent sections, which deal with, respectively, global analysis in 1-D (§3), pointwise analysis in higher dimensions (§4), and global analysis in higher dimensions (§5). In §6 we discuss possible avenues by which this analysis can be extended to non-uniform meshes, such as may be obtained in Lagrangian or adaptive mesh refinement (AMR) calculations. We exercise this process on a selected number of problems of relevance to the ASC V&V community in §7,

demonstrating aspects of problem complexity on the fidelity of the metrics. We summarize the contents of this report in §8.

2 Pointwise Convergence Analysis in 1-D

In this section, we lay out the fundamental notions regarding convergence analysis in the simplest scenario: pointwise comparison of quantities in one spatial dimension. For any variable ξ computed at a given *uniform* grid spacing Δx_i and *uniform* timestep Δt_l, the fundamental *Ansatz* of pointwise convergence analysis is that the difference between the exact and computed solutions can be expanded as a function of the spatial and temporal zone sizes:

$$\begin{aligned} \xi^* - \xi_i^l = \mathcal{E}_0 + \mathcal{A}\,(\Delta x_i)^p + \mathcal{B}\,(\Delta t_l)^q + \mathcal{C}\,(\Delta x_i)^r\,(\Delta t_l)^s \\ + o\Big((\Delta x_i)^p, (\Delta t_l)^q, (\Delta x_i)^r\,(\Delta t_l)^s\Big), \end{aligned} \tag{1}$$

where ξ^* is the *exact* value, ξ_i^l is the value computed on the grid of spatial zone size Δx_i and timestep Δt_l, $\mathcal{E}_0$ is the *zeroth-order error*, $\mathcal{A}$ is the *spatial convergence coefficient*, p is the *spatial convergence rate*, $\mathcal{B}$ is the *temporal convergence coefficient*, q is the *temporal convergence rate*, $\mathcal{C}$ is the *spatio-temporal convergence coefficient*, and $r + s$ is the *spatio-temporal convergence rate*. By the notation "$o\Big((\Delta x_i)^p, (\Delta t_l)^q, (\Delta x_i)^r\,(\Delta t_l)^s\Big)$" we mean terms that approach zero faster than $(\Delta x_i)^p$, $(\Delta t_l)^q$, and $(\Delta x_i)^r\,(\Delta t_l)^s$ as both Δx_i and Δt_l becomes vanishingly small (i.e., as Δx_i, $\Delta t_l \rightarrow 0^+$). In the following, we also refer to these vanishingly small terms as "higher order terms" or H.O.T.

There are four canonical cases, depending on the relative magnitudes of various parameters in Eq. 1.

- $|\mathcal{E}_0| \gg |\mathcal{A}\,(\Delta x_i)^p|$, $|\mathcal{B}\,(\Delta t_l)^q|$, $|\mathcal{C}\,(\Delta x_i)^r\,(\Delta t_l)^s|$. In this case, there is zeroth-order convergence, i.e., the error is independent of both the spatial grid size and the timestep.
- $p < q$, $r + s$ with $\mathcal{E}_0 = 0$. In this case, the convergence is dominated by *spatial* errors.
- $q < p$, $r + s$ with $\mathcal{E}_0 = 0$. In this case, the convergence is dominated by *temporal* errors.
- $p \approx q \cong r + s$ or $p \approx q \leq r + s$ or $r + s \leq p$, q, all with $\mathcal{E}_0 = 0$. In this case, the convergence is dominated by mixed, *spatio-temporal* errors.

Numerical methods commonly used in hydrocodes are constructed from fundamental algorithms that are typically either first or second order in space and time for smooth problems.[1]

[1] Some higher-than-second-order spatial methods are being implemented in certain codes.

Pointwise convergence analysis can be performed for a variable defined at each point in a computational grid, e.g., a field variable (such as density), in which case convergence parameters are obtained throughout the computational grid. Importantly, pointwise convergence analysis in 1-D can also be performed on a functional of the computed solution, e.g., a quantity defined in terms of values computed at each point of the computational grid (e.g., total kinetic energy) or an algorithmically defined local feature (e.g., shock position). This consideration also applies to the comparison of computed cell-averaged quantities (such as are employed in certain algorithms) with their appropriately evaluated exact solution counterparts. In this case, a set of convergence parameters related to such quantity is obtained for the support of that functional, which may be a strict subset of the entire computational grid.

2.1 Pointwise Spatial Convergence Analysis in 1-D

Experience with spatial and temporal integrators indicates that the spatial error is often much greater than the temporal error for the numerical integration of spatial- and time-dependent PDEs dominated by hyperbolic behavior. In other circumstances, this is not the case. In the following analysis, we assume this to be true, so that the following relation holds:

$$\mathcal{E}_{x_i} \equiv |\mathcal{A}\ (\Delta x_i)^p\ | \ > |\mathcal{B}\ (\Delta t_l)^q\ | \equiv \mathcal{E}_{t_l}. \tag{2}$$

The opposite case is discussed in §2.2, and the more general case of simultaneous spatio-temporal convergence is described in §2.3.

To determine the parameters in these expressions, we eliminate $\mathcal{E}_0$ in the *Ansatz*; we may do this without loss of generality, for, if a zeroth-order error exists, this behavior will be manifested in the solution for the other order parameters. Restricting the *Ansatz* of Eq. 1 to spatial convergence only, we suppress the temporal index l, and assume that

$$\xi^* - \xi_i = \mathcal{A}\ (\Delta x_i)^p + \text{H.O.T.}. \tag{3}$$

For the solution on a "coarse" grid, denoted with the subscript c, $\Delta x_c \equiv \Delta x$, and Eq. 3 implies

$$\xi^* - \xi_c = \mathcal{A}\ (\Delta x)^p + \cdots . \tag{4}$$

Consider now the computed solution on a less-coarse, i.e., "medium", grid with cell size Δx_m such that $\Delta x_c/\Delta x_m = \Delta x/\Delta x_m \equiv \sigma > 1$, i.e., $\Delta x_m = \Delta x_c/\sigma = \Delta x/\sigma$. In many applications, $\sigma = 2$, corresponding to "halving" the grid; while this value of σ is often used, it need not necessarily be set to this value. For this solution, Eq. 3 implies

$$\xi^* - \xi_m = \sigma^{-p}\,\mathcal{A}\ (\Delta x)^p + \cdots . \tag{5}$$

2.1.1 1-D Pointwise Spatial Convergence, Exact Solution Known

Let us now assume that we know *a priori* the exact solution ξ^* at any location. With this assumption, Eqs. 4 and 5 form a system of two equations in the two unknowns $\mathcal{A}$ and p. This system can be solved explicitly for these quantities:

$$\boxed{\begin{aligned} p &\equiv [\log(\xi^* - \xi_c) - \log(\xi^* - \xi_m)] / \log \sigma \,, \\ \mathcal{A} &\equiv (\xi^* - \xi_c) / (\Delta x)^p \,. \end{aligned}} \tag{6}$$

Obtaining these values, the convergence rate p and convergence coefficient $\mathcal{A}$, represents the essence of verification analysis. These two scalars constitute *metrics*, available at each zone on the coarse grid, that provide unambiguous local measures of the code (i.e., algorithm) convergence properties. It is important to note that these metrics are computed at each *coarse* grid location; the relationship of the coarse and medium grids is discussed further in §2.1.4

2.1.2 1-D Pointwise Spatial Convergence, No Exact Solution

We now assume that we *do not* (or, perhaps, *cannot*) know the exact solution ξ^* at any location. In this case, we cannot measure the *absolute* local convergence properties of the algorithm; we can, however, quantify the *relative* local convergence properties, namely the *self-convergence* behavior of the algorithm. This procedure forms the basis of *calculation verification*, which is the process whereby one demonstrates convergence of a calculation in configurations for which no exact solution exists. Such cases occur, e.g., where complex geometry exists or when the equations contain multiple mathematical operators, representing interacting physical processes.

In this case, Eqs. 4 and 5 now form a system of two equations in three unknowns: $\mathcal{A}$, n, and the unknown solution value ξ^*. Unlike the previous case, we now additionally consider the solution on a "fine" grid with uniform zone size Δx_f, for which $\Delta x_m / \Delta x_f \equiv \tau > 1$, i.e., $\Delta x_f = \Delta x_m / \tau = \Delta x_c / (\sigma\tau)$. As with σ, in practice τ often assumes the value two, though this need not necessarily be so. For this solution, Eq. 3 implies

$$\xi^* - \xi_f = \sigma^{-p} \, \tau^{-p} \, \mathcal{A} \, (\Delta x)^p + \cdots \tag{7}$$

Equations 4, 5, and 7 form a system of three equations in the three unknowns $\mathcal{A}$, p, and ξ^*. Taking the difference of Eqs. 4 and 5 implies that

$$\xi_m - \xi_c = \mathcal{A} \, (\Delta x)^p \, \left(1 - \sigma^{-p}\right) \,; \tag{8}$$

similarly, the difference of Eqs. 5 and 7 yields

$$\xi_f - \xi_m = \sigma^{-p} \, \mathcal{A} \, (\Delta x)^p \, \left(1 - \tau^{-p}\right) \,. \tag{9}$$

Taking the ratio of these last two expressions yields

$$\frac{\xi_m - \xi_c}{\xi_f - \xi_m} = \frac{\sigma^p - 1}{1 - \tau^{-p}} \,. \tag{10}$$

This is a nonlinear equation in one unknown, p, that can be solved numerically (i.e., *not* analytically) at each point on the coarse grid. Once that value is calculated, the convergence coefficient can be evaluated at each location by taking the difference of Eqs. 8 and 9 and solving for $\mathcal{A}$ to obtain:

$$\mathcal{A} = - \frac{\xi_f - 2\xi_m + \xi_c}{(\Delta x)^p \, [(1 - \sigma^{-p}) - \sigma^{-p} \, (1 - \tau^{-p})]} \,. \tag{11}$$

Significant simplification is possible if we assume that $\sigma = \tau$, i.e., that the ratio of grid spacing between the medium and coarse grids equals the ratio of grid spacing between the fine and medium grids. In this case, Eq. 10 simplifies to

$$\frac{\xi_m - \xi_c}{\xi_f - \xi_m} = \sigma^p \,, \tag{12}$$

which can be solved explicitly for the convergence rate p:

$$\boxed{p = [\log(\xi_m - \xi_c) - \log(\xi_f - \xi_m)] \,/ \log \sigma \,.} \tag{13}$$

Eq. 11 for the convergence coefficient simplifies to

$$\boxed{\mathcal{A} = - \, (\, \xi_f - 2\xi_m + \xi_c \,) \, \Big/ \left[\, (\Delta x)^p \, (1 - \sigma^{-p})^2 \, \right] \,.} \tag{14}$$

The two scalars in Eqs. 13 and 14 are, again, convergence metrics, available at each point in the coarse computational grid, that quantify the self-convergence properties of the underlying numerical algorithm.

2.1.3 1-D Mean Pointwise Spatial Convergence

The above expressions provide *pointwise* values of the two metrics given by the convergence coefficient $\mathcal{A}$ and convergence rate p. To obtain a more extensive metric, one can construct, e.g., mean values of these convergence parameters over a given spatial interval. For example, a mean convergence rate over the entire domain is constructed by taking the arithmetic average of the (local) convergence rate at each gridpoint, i.e.,

$$\hat{p} = \frac{1}{\hat{N}} \sum_i p_i \,, \tag{15}$$

where p_i is the asymptotic convergence rate computed at gridpoint x_i, $i = 1, \ldots, \hat{N}$. We indicate the total number of points in this average as $\hat{N}$ and

not as N, since all points on the computational grid might not be used in the evaluation of the mean pointwise convergence rate [3, 7, 8]. For example, if the numerical values of the cell-averaged quantities from the fine and medium meshes are identical, then the expression for n in Eq. 13 either diverges (if those values do not equal the value on the coarse mesh) or is undefined (if all values are identical). Similarly, the computed value of the argument of the logarithm in the numerator of Eq. 13 could be negative, leading to an imaginary value for p. Therefore, one should include only well-defined pointwise convergence rates in Eq. 15, so that, in general, $\hat{N} \neq N$.

In addition to the statistic given by Eq. 15, further characterization of the distribution of convergence rates over the mesh is give by the sample variance of these values:

$$\mathrm{Var}(p_1, \ldots, p_{\hat{N}}) = \frac{1}{\hat{N} - 1} \sum_i (p_i - \hat{p}) \,. \tag{16}$$

The standard deviation of convergence rates can be computed as the square root of this quantity. Higher moments by which to characterize the distribution can be similarly evaluated.

2.1.4 Comment: Values at Identical Space-time Locations

Implicit in the preceding manipulations of pointwise values are the assumptions that the results are (1) spatially located at identical gridpoints and (2) at the same time. Empirical evidence suggests that convergence results depend sensitively on these constraints; that is, applying the above analysis to values that are not spatially and temporally co-located may result in erroneous or misleading convergence results.

If the computational mesh is such that the points on the corresponding grids under consideration are *not* at the identical positions, then spatial interpolation must be performed. For example, assume that the ratio of grid sizes is taken to be two, in which case the following procedure applies. The spatially-weighted means of the two bracketing values of the medium solution and the four bracketing values of the fine solution are calculated and used to obtain the cell-averaged values at the corresponding coarse gridpoint. Using density as the variable of interest and assuming the coarse grid has N points, values $\rho^m_{i'}$ from the i'th zone (which has spatial extent $V^m_{i'}$ [i.e., length in 1-D, area in 2-D, or volume in 3-D]) of the medium-grid solution, $i' = 1, \ldots, 2N$, are interpolated to the value $\rho^{c \leftarrow m}_i$ at locations x_i, $i = 1, \ldots, N$, on the coarse grid as

$$\rho^{c \leftarrow m}_i = \left(V^m_{2i-1} \rho^m_{2i-1} + V^m_{2i} \rho^m_{2i} \right) / \left(V^m_{2i-1} + V^m_{2i} \right) \,. \tag{17}$$

Similarly, values from the fine solution, $\rho^f_{\hat{\imath}}$, $\hat{\imath} = 1, \ldots, 4N$, are interpolated to the locations $\rho^{c \leftarrow f}_i$ at the corresponding position on the coarse grid as

$$\rho^{c \leftarrow f}_i = \frac{V^f_{4i-3} \rho^f_{4i-3} + V^f_{4i-2} \rho^f_{4i-2} + V^f_{4i-1} \rho^f_{4i-1} + V^f_{4i} \rho^f_{4i}}{V^f_{4i-3} + V^f_{4i-2} + V^f_{4i-1} + V^f_{4i}} \,. \tag{18}$$

These values are used in Eq. 13 and 14 to determine the pointwise convergence characteristics.

2.1.5 Comment: Review of Assumptions

It is important to review the assumptions embedded in the general error *Ansatz* of Eq. 1. First, the algorithm's total discretization error is assumed to be the summation of independent terms. For PDEs that discretize both the space and time continua, this assumption is frequently confirmed through rigorous verification studies. This assumption, however, is not universally true for all existing (or future) numerical methods. The form and functionality of the error *Ansatz* must, therefore, also be confirmed through the verification process. Second, all solution calculations must fall within the regime of validity of the spatial and temporal asymptotic behavior encapsulated in the error *Ansatz*. This tacitly requires that any associated initial or boundary conditions be consistent with this assumption.

An additional assumption is invoked for conducting verification studies intended to elicit either the spatial convergence metrics alone or the temporal convergence metrics alone *but not both simultaneously*. This third assumption is that the error-of-interest either dominates or can be separated from all other discretization errors. For example, spatial convergence analysis using Eq. 3 assumes that the temporal error is much smaller than the spatial error. As discussed in the following section, a similar error *Ansatz* can be made for temporal convergence, using either the assumption that the spatial error is negligible but unknown or that the spatial error dominates but has known behavior. To our knowledge there exists no method by which to ensure the relative levels of discretization error prior to commencing any such analysis. There is, however, a simple methodology for conducting separate spatial or temporal convergence analysis that acknowledges the three assumptions described above.

For example, for 1-D pointwise spatial convergence analysis when no exact solution is known, a minimum of three simulations are required to compute the convergence metrics in Eqs. 13 and 14. A series of three calculations, each with unique spatial zoning, is required. In contrast, an identical timestep is commonly used for each simulation in the convergence series. Furthermore, this timestep is generally held constant throughout each simulation. This practice, viz., using an identical and constant timestep, represents a conservative strategy for the timestep because the only assumption placed on Δt in Eq. 3 is that the temporal discretization error be negligibly small relative to the spatial error. By enforcing that each simulation use the same, constant timestep, one attempts to ensure that the simulation series uniformly satisfies this assumption.

This situation is depicted in the schematic in Fig. 1, which contains a plotted idealization of the error as a function of the spatial grid size for a set of three simulations. The symbols identify the errors ($E_{x,c} > E_{x,m} > E_{x,f}$) associated with each calculation (on grids of zone size $\Delta x_c > \Delta x_m > \Delta x_f$). The solid line

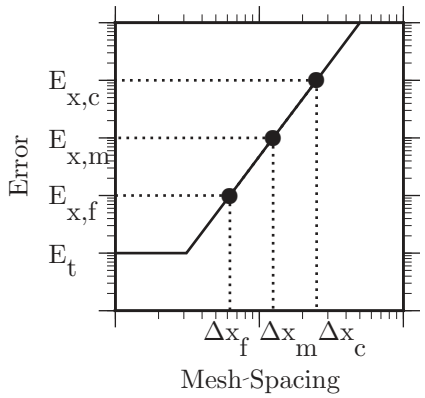

Figure 1: Schematic plot of the computational error plotted against the spatial grid size for a set of three simulations, all conducted with the same timestep. The symbols identify the errors associated with each calculation. The solid line represents the error of the calculations across the continuum of possible mesh spacings.

represents the error of the calculations across the continuum of possible mesh spacings. The behavior depicted in this figure is predicated upon the assumptions that the spatial error of the simulations is greater than the temporal error (E_t) and that the spatial and temporal errors are separable to leading order. This plot suggests that the approach described above is valid for simulations so long as the temporal error is less than the spatial error. More specifically, the timestep need not necessarily be kept constant, provided that the greatest temporal error from any simulation considered is less than the smallest spatial error.

From these simulations (i.e., with three distinct spatial zonings and one uniform timestep), the convergence metrics are computed using Eqs. 13 and 14. Additional simulations, however, may also be required, e.g., if the initial algorithmic convergence rate does not approach the theoretical value; this can happen, e.g., if one is not within the range of asymptotic validity of the error *Ansatz* for the algorithm or if the solution under investigation does not comply with the requirements for the theoretical convergence behavior (e.g, the solution contains discontinuous features). From these subsequent simulations, together with the three initial simulations, multiple convergence coefficients and rates are then computed and compared. The entire verification analysis is completed and the convergence metrics are established only when these metrics are unchanging in this iterative process: one is then in asymptotic range of validity of the fundamental error *Ansatz*. If such an iterative verification process fails to agree with the theoretical estimates or fails to converge, then one must revisit

the software implementation and, perhaps, the mathematical foundation of the algorithm.

2.2 Pointwise Temporal Convergence Analysis in 1-D

For the algorithms and discretization parameters chosen, the temporal error may dominate the spatial error. If this is the case, then the requisite temporal convergence analysis is exactly analogous to spatial convergence analysis presented in the previous section. Quantitative measures of temporal convergence are given, e.g., by the analogues of Eqs. 6, 13, and 14.

We now assume the typical case, with dominant spatial error. Under this assumption, quantitative estimates of the spatial error can be obtained. The general error *Ansatz* of Eq. 1 can be re-written as

$$\xi^* - \xi_i^l - \mathcal{E}_x = \mathcal{B}\ (\Delta t_l)^q + \text{H.O.T.}\,, \tag{19}$$

where $\mathcal{E}_x = \mathcal{A}\ (\Delta x)^p$ represents the corresponding spatial error, and we have absorbed any possible constant error into the time-dependent term.

2.2.1 Pointwise Temporal Convergence: Exact Solution Known

With a solution on a "coarse" temporal grid, with $\Delta t = \Delta t_c$, and a solution on a "medium" temporal grid, with $\Delta t_m = \Delta t_c/\tau$ for some $\tau > 1$, one can solve for the convergence parameters q and $\mathcal{B}$ as

$$\boxed{\begin{array}{rcl} q & \equiv & \left[\log\left(\xi^* - \xi_c - \mathcal{E}_x^c\right) - \log\left(\xi^* - \xi_m - \mathcal{E}_x^m\right)\right] / \log\tau\,, \\ \mathcal{B} & \equiv & \left(\xi^* - \xi_c - \mathcal{E}_x^c\right) / (\Delta t)^q\,. \end{array}} \tag{20}$$

Three observations regarding these results are warranted. First, an identical *spatial* grid is used in both of these calculations, which are on "coarse" and "medium" *temporal* grids. Second, one must first have performed the corresponding spatial convergence analysis to obtain estimates of $\mathcal{E}_x^c$ and $\mathcal{E}_x^m$, which, despite being indexed as such, are presumably independent of the timestep. And third, the identical test probem is used for *all* the calculations used in these spatial and temporal convergence analyses.

2.2.2 Pointwise Temporal Convergence: Exact Solution Unknown

If no exact solution is available, then we use a fine grid solution in its place. Under the assumptions analogous to those mentioned above, this case leads to the following estimates of the (self-)convergence metrics:

$$\boxed{\begin{array}{rcl} q & \equiv & \left[\log\left(\xi^f - \xi_c - \mathcal{E}_x^c\right) - \log\left(\xi^f - \xi_m - \mathcal{E}_x^m\right)\right] / \log\tau\,, \\ \mathcal{B} & \equiv & \left(\xi^f - \xi_c - \mathcal{E}_x^c\right) / (\Delta t)^q\,. \end{array}} \tag{21}$$

2.3 Pointwise Spatio-temporal Convergence Analysis in 1-D

The analysis for simultaneous spatio-temporal convergence is significantly more complicated than the previous cases. In the case of a known exact solution, the simplest form of the *Ansatz* given in Eq. 1 for spatio-temporal convergence contains four unknowns ($\mathcal{A}$, p, $\mathcal{B}$, and q), while the case of an unknown exact solution contains five unknowns (the previous four plus the exact solution ξ^*). Here, we tacitly assume that the individual spatial and temporal error terms dominate the mixed spatio-temporal term. To solve for these unknowns, one must have an identical number of equations, each of which contains computed solution values. The resulting set of four or five equations cannot be solved in closed form, even for the case of uniform zoning ratios. To solve for the convergence parameters, therefore, one must resort to numerical methods for finding the solutions of a set of coupled nonlinear equations. Anecdotally, we have found the numerical solution of these sets of equations to be fairly sensitive to, e.g., the initial solution guess. In the following sections, we outline possible solution procedures in these cases.

2.3.1 1-D Pointwise Spatio-Temporal Convergence, Exact Solution Known

Let us now assume that we know *a priori* the exact solution ξ^* at any location. As stated above, we restrict ourselves to the case with $p,\ q \leq r + s$ (see the *Ansatz* and description on p. 2). With these assumptions, we obtain computed solutions with the following four combinations of spatial and temporal zoning: $\{\Delta x, \Delta t\}$, $\{\Delta x/\sigma, \Delta t\}$, $\{\Delta x, \Delta t/\tau\}$, and $\{\Delta x/\sigma, \Delta t/\tau\}$. From Eq. 1, these solutions satisfy the following equalities:

$$\begin{aligned}
\xi^* - \xi_1 &= \quad \mathcal{A}\,(\Delta x)^p + \quad \mathcal{B}\,(\Delta t)^q + \cdots, \\
\xi^* - \xi_2 &= \mathcal{A}\,(\Delta x/\sigma)^p + \quad \mathcal{B}\,(\Delta t)^q + \cdots, \\
\xi^* - \xi_3 &= \quad \mathcal{A}\,(\Delta x)^p + \mathcal{B}\,(\Delta t/\tau)^q + \cdots, \\
\xi^* - \xi_4 &= \mathcal{A}\,(\Delta x/\sigma)^p + \mathcal{B}\,(\Delta t/\tau)^q + \cdots.
\end{aligned} \tag{22}$$

These equations form the system of four equations in the four unknown $\mathcal{A}$, $\mathcal{B}$, p, and q. The subsequent algebra can be simplified somewhat by considering the following linear combinations of the first and second, and first and third of these equations:

$$\xi_2 - \xi_1 = \left(1 - \sigma^{-p}\right)\,\mathcal{A}\,(\Delta x)^p + \cdots \tag{23}$$

$$\xi_3 - \xi_1 = \left(1 - \tau^{-q}\right)\,\mathcal{B}\,(\Delta t)^q + \cdots \tag{24}$$

We consider the system of four equations given by the first and last equations in Eq. 22 together with the above two equations. These relations are considered to depend on the variable $\mathbf{a} \equiv [a_1, a_2, a_3, a_4]^T \equiv [\mathcal{A}, p, \mathcal{B}, q]^T$:

$$
\begin{aligned}
f_1(\mathbf{a}) = &\quad a_1\,(\Delta x)^{a_2} + &&\quad a_3\,(\Delta t)^{a_4} - (\xi^* - \xi_1) = 0\,,\\
f_2(\mathbf{a}) = &\quad \sigma^{-a_2}\,a_1\,(\Delta x)^{a_2} + &&\quad \tau^{-a_4}\,a_3\,(\Delta t)^{a_4} - (\xi^* - \xi_4) = 0\,,\\
f_3(\mathbf{a}) = &\quad (1-\sigma^{-a_2})\,a_1\,(\Delta x)^{a_2} &&\quad - (\xi_2 - \xi_1) = 0\,,\\
f_4(\mathbf{a}) = &\quad &&\quad (1-\tau^{-a_4})\,a_3\,(\Delta t)^{a_4} - (\xi_3 - \xi_1) = 0\,.
\end{aligned}
\tag{25}
$$

The typical method of solution of the set of nonlinear equations $\mathbf{f}(\mathbf{a}) = \mathbf{0}$ is Newton's method or some variant thereof. The basic Newton iteration estimate of the k-th iterative approximation $\mathbf{a}^k$ to the solution is

$$
\mathbf{a}^k = \mathbf{a}^{k-1} - \left(\frac{\partial \mathbf{f}}{\partial \mathbf{a}}\right)^{-1}\Bigg|_{\mathbf{a}^{k-1}} \mathbf{f}(\mathbf{a}^{k-1})\,. \tag{26}
$$

The Jacobian $\partial\mathbf{f}/\partial\mathbf{a}$, the inverse of which is typically evaluated numerically, is given below for the above set of equations:

$$
\begin{pmatrix}
(\Delta x)^{a_2} & a_1\,(\Delta x)^{a_2}\log\Delta x & (\Delta t)^{a_4} & a_3\,(\Delta t)^{a_4}\log\Delta t \\
\sigma^{-a_2}\,(\Delta x)^{a_2} & a_1\sigma^{-a_2}\,(\Delta x)^{a_2} \times [\log\Delta x - \log\sigma] & \tau^{-a_4}\,(\Delta t)^{a_4} & a_3\tau^{-a_4}\,(\Delta t)^{a_4} \times [\log\Delta t - \log\tau] \\
(1-\sigma^{-a_2})\,(\Delta x)^{a_2} & a_1(\Delta x)^{a_2}\big[\sigma^{-a_2}\log\sigma + (1-\sigma^{-a_2})\log\Delta x\big] & 0 & 0 \\
0 & 0 & (1-\tau^{-a_4})\,(\Delta t)^{a_4} & a_3(\Delta t)^{a_4}\big[\tau^{-a_4}\log\tau + (1-\tau^{-a_4})\log\Delta t\big]
\end{pmatrix}.
\tag{27}
$$

One difficulty involved in solving Eq. 25 is assigning an initial guess that is within the domain of convergence of the iteration. An additional issue is the possibility of obtaining multiple solutions to this set of nonlinear equations. These issues must be dealt with on a case-by-case basis.

2.3.2 1-D Pointwise Spatio-Temporal Convergence, Exact Solution Unknown

In this case, Eq. 1 contains five unknown quantities: $\mathcal{A}$, $\mathcal{B}$, p, q, and the exact solution ξ^*. A nonsingular system of five results may obtained by using solutions computed with the following pairs of spatial zoning: $\{\Delta x, \Delta t\}$, $\{\Delta x/\sigma, \Delta t\}$, $\{\Delta x, \Delta t/\tau\}$, $\{\Delta x/\sigma, \Delta t/\tau\}$, and $\{\Delta x/\sigma^2, \Delta t\}$. These solutions satisfy the following equalities:

$$
\begin{aligned}
\xi^* - \xi_1 &= \quad \mathcal{A}\,(\Delta x)^p + \quad \mathcal{B}\,(\Delta t)^q + \cdots,\\
\xi^* - \xi_2 &= \mathcal{A}\,(\Delta x/\sigma)^p + \quad \mathcal{B}\,(\Delta t)^q + \cdots,\\
\xi^* - \xi_3 &= \quad \mathcal{A}\,(\Delta x)^p + \mathcal{A}\,(\Delta t/\tau)^q + \cdots,\\
\xi^* - \xi_4 &= \mathcal{A}\,(\Delta x/\sigma)^p + \mathcal{A}\,(\Delta t/\tau)^q + \cdots.\\
\xi^* - \xi_5 &= \mathcal{A}\left(\Delta x/\sigma^2\right)^p + \quad \mathcal{B}\,(\Delta t)^q + \cdots,
\end{aligned}
\tag{28}
$$

The subsequent algebra can be simplified somewhat by considering the following linear combinations of the first and second, first and third, and first and fifth of these equations:

$$\xi_2 - \xi_1 = \left(1 - \sigma^{-p}\right) \mathcal{A} \left(\Delta x\right)^p + \cdots \tag{29}$$

$$\xi_3 - \xi_1 = \left(1 - \tau^{-q}\right) \mathcal{B} \left(\Delta t\right)^q + \cdots \tag{30}$$

$$\xi_5 - \xi_1 = \left(1 - \sigma^{-2p}\right) \mathcal{A} \left(\Delta x\right)^p + \cdots . \tag{31}$$

Consider the system of five equations given by the first and last equations in Eq. 28 together with the above three equations. These relations are considered to depend on the variable $\mathbf{a} \equiv [a_1, a_2, a_3, a_4, a_5]^T \equiv [\mathcal{A}, p, \mathcal{B}, q, \xi^*]^T$:

$$\begin{aligned}
f_1(\mathbf{a}) &= a_1 \left(\Delta x\right)^{a_2} + a_3 \left(\Delta t\right)^{a_4} - \left(a_5 - \xi_1\right) = 0 \,, \\
f_2(\mathbf{a}) &= \sigma^{-a_2} a_1 \left(\Delta x\right)^{a_2} + \tau^{-a_4} a_3 \left(\Delta t\right)^{a_4} - \left(a_5 - \xi_4\right) = 0 \,, \\
f_3(\mathbf{a}) &= \left(1 - \sigma^{-a_2}\right) a_1 \left(\Delta x\right)^{a_2} - \left(\xi_2 - \xi_1\right) = 0 \,, \\
f_4(\mathbf{a}) &= \left(1 - \tau^{-a_4}\right) a_3 \left(\Delta t\right)^{a_4} - \left(\xi_3 - \xi_1\right) = 0 \,. \\
f_5(\mathbf{a}) &= \left(1 - \sigma^{-2a_2}\right) a_1 \left(\Delta x\right)^{a_2} - \left(\xi_5 - \xi_1\right) = 0 \,,
\end{aligned} \tag{32}$$

As in the previous section, Newton's method can be used to solve this nonlinear set of equations. The Jacobian of this set of equations is more complex than in the previous case. This derivation illustrates the even greater complexity of this case and provides the basis by which to implement this analysis, for which we know of no published results.

3 Global Convergence Analysis in 1-D

For global convergence analysis, we make the *Ansatz* that the *norm* of the difference between the exact and computed solutions can be expanded as a function of the spatial and temporal zone sizes:

$$||\xi^* - \xi_i^l|| = \mathcal{A} \left(\Delta x_i\right)^p + \mathcal{B} \left(\Delta t_l\right)^q + o\Big(\left(\Delta x_i\right)^p, \left(\Delta t_l\right)^q\Big) \,, \tag{33}$$

where, again, ξ^* is the *exact* value, ξ_i^l is the value computed on the grid of spatial zone size Δx_i and timestep Δt_l, $\mathcal{A}$ and p are the spatial convergence coefficient and rate, and $\mathcal{B}$ and q are the temporal convergence coefficient and rate. Following the discussion of §2, here we neglect the constant and mixed error terms present in the more general *Ansatz* corresponding to Eq. 1. In Eq. 33 we are making an assumption regarding a non-local relation between the exact and computed solutions. We discuss below the implications of using the non-local norm, which characterizes the global behavior, in this equation.

3.1 Definition of Norms in 1-D

The standard definition for the L_p functional norm of the function f defined on the interval $[a, b]$ is

$$||f||_p \equiv \left[\int_a^b dx \, |f(x)|^p \right]^{1/p} . \tag{34}$$

Based on this definition, the L_1, L_2, and L_∞ norms are defined as

$$||f||_1 \equiv \int_a^b dx \, |f(x)| , \tag{35}$$

$$||f||_2 \equiv \sqrt{\int_a^b dx \, |f(x)|^2} , \quad \text{and} \tag{36}$$

$$||f||_\infty \equiv \max_{x \in [a,b]} |f(x)| . \tag{37}$$

Note that the L_∞ norm is independent of any integral and is straightforward to evaluate numerically.

To approximate the integral on the interval $[a, b]$, assume that there are N points x_i, $i = 1, \ldots, N$, each being the center of a zone of length Δx_i. Then, the simplest quadrature scheme is to approximate the the integral as follows:

$$\int_a^b dx \, g(x) \doteq \sum_{i=1}^{N} g(x_i) \, \Delta x_i . \tag{38}$$

With this assumption, the L_1 and L_2 norms become:

$$||f||_1 \equiv \sum_{i=1}^{N} |f(x_i)| \, \Delta x_i , \tag{39}$$

$$||f||_2 \equiv \sqrt{\sum_{i=1}^{N} |f(x_i)|^2 \, \Delta x_i} . \tag{40}$$

For uniform zoning, $\Delta x_i \equiv \Delta x = (b - a)/N$, and the above approximations simplify further:

$$||f||_1 \equiv \Delta x \sum_{i=1}^{N} |f(x_i)| , \tag{41}$$

$$||f||_2 \equiv \sqrt{\Delta x \sum_{i=1}^{N} |f(x_i)|^2} . \tag{42}$$

3.2 Global Spatial Convergence Analysis in 1-D

Restricting the global *Ansatz* of Eq. 33 to spatial convergence only, we again assume that the spatial error is dominant, which is often the case. Suppressing the temporal index l, we assume that

$$||\xi^* - \xi_i|| = \mathcal{A}\ (\Delta x_i)^p + o\Big((\Delta x_i)^p\Big)\,. \tag{43}$$

For the solution on a coarse grid, denoted with the subscript c, $\Delta x_c \equiv \Delta x$ and Eq. 3 implies

$$||\xi^* - \xi_c|| = \mathcal{A}\ (\Delta x)^p + \cdots\,. \tag{44}$$

Consider now the computed solution on a less-coarse, i.e., medium, grid, so that $\Delta x_c/\Delta x_m = \sigma > 1$, i.e., $\Delta x_m = \Delta x_c/\sigma$. For this solution,

$$||\xi^* - \xi_m|| = \sigma^{-p}\,\mathcal{A}\ (\Delta x)^p + \cdots\,. \tag{45}$$

3.2.1 1-D Global Spatial Convergence, Exact Solution Known

Assume that one can calculate *a priori* the exact solution ξ^* at any location. With this assumption, the norms of the differences on the left-hand side (LHS) of Eqs. 44 and 45 can be calculated, since ξ^*, ξ_c, and ξ_m are known at the quadrature points, so that the norms can be evaluated explicitly. Eqs. 44 and 45 form a system of two equations in the two unknowns $\mathcal{A}$ and p. This system can be solved explicitly for these quantities:

$$\boxed{\begin{array}{rcl} p & \equiv & \big[\log||\xi^* - \xi_c|| - \log||\xi^* - \xi_m||\,\big]\big/\log\sigma\,, \\ \mathcal{A} & \equiv & ||\xi^* - \xi_c||\,/\,(\Delta x)^p\,. \end{array}} \tag{46}$$

These two scalar metrics quantify the global convergence characteristics of a given numerical algorithm.

3.2.2 1-D Global Spatial Convergence, No Exact Solution

As in §2.1.2, we again assume that we *do not* (or, perhaps, *cannot*) know the exact solution ξ^* at any location. Such is the case in *calculation verification*, as mentioned above. Eqs. 44 and 45 now form a system of two equations in three unknowns: $\mathcal{A}$, n, and the unknown solution value ξ^*. Without the exact solution, we cannot evaluate the norms on the LHS of these equations. As in the pointwise case, we must use an approximation to the exact solution, which we take to be the solution on a fine grid; using this solution, we are effectively characterizing the self-convergence of the underlying algorithm. In this case, we modify the standard convergence *Ansatz* of Eq. 43 to be

$$||\xi_f - \xi_i|| = \mathcal{A}\ (\Delta x_i)^p + o\Big((\Delta x_i)^p\Big)\,. \tag{47}$$

That is, we substitute ξ_f for ξ^* in Eqs. 44 and 45. Those equations form a system of two equations in the two unknowns $\mathcal{A}$ and p. That system has the solution given as:

$$\boxed{\begin{array}{rcl} p & \equiv & \left[\log ||\xi_f - \xi_c|| - \log ||\xi_f - \xi_m|| \right] / \log \sigma \,, \\ \mathcal{A} & \equiv & ||\xi_f - \xi_c|| \,/\, (\Delta x)^p \,. \end{array}} \tag{48}$$

3.2.3 Comment: Identical Space-time Locations and Timesteps

The issues raised in §§2.1.4 and 2.1.5 apply as well in the present case of global convergence analysis. Specifically, the computed data being analyzed must be at locations and times that are identical to (approximately) machine precision; otherwise, the convergence analysis can produce meaningless results. Additionally, the underlying assumption is that the spatial discretization and timestep yield temporal errors that are negligible compared to the spatial errors in all computed solutions. A conservative strategy by which this may be achieved is to keep the timestep identical and constant for all simulations. Refer to §2.1.5 for a further discussion of these issues.

3.3 Global Temporal Convergence Analysis in 1-D

The global analysis in the previous section can be combined with the temporal convergence analysis of §2.2 to obtain global temporal convergence parameters. This analysis is based on the assumption that the the spatial error dominates the temporal error for the algorithm and discretization parameters chosen. In the next two subsections, we present the results for the convergence parameters without derivation.

3.3.1 1-D Global Temporal Convergence, Exact Solution Known

If an exact solution is known, then the analysis outlined in §2.2.1 can be followed to obtain the results in this case. We provide the following results without derivation:

$$\boxed{\begin{array}{rcl} q & \equiv & \left[\log \left(||\xi^* - \xi_c|| - \mathcal{E}_x^c \right) - \log \left(||\xi^* - \xi_m|| - \mathcal{E}_x^m \right) \right] / \log \tau \,, \\ \mathcal{B} & \equiv & \left(||\xi^* - \xi_c|| - \mathcal{E}_x^c \right) / (\Delta t)^q \,. \end{array}} \tag{49}$$

3.3.2 1-D Global Temporal Convergence, No Exact Solution

If an exact solution is not known, we use a solution on a fine grid as the fiducial exact solution and modify the error *Ansatz* accordingly. This leads to the

following expressions for the convergence parameters:

$$\boxed{\begin{array}{rcl} q & \equiv & \left[\log\left(||\xi^f - \xi^c|| - \mathcal{E}_x^c \right) - \log\left(||\xi^f - \xi^m|| - \mathcal{E}_x^m \right) \right] / \log \tau \,, \\ \mathcal{B} & \equiv & \left(||\xi^f - \xi^c|| - \mathcal{E}_x^c \right) / \left(\Delta t \right)^q \,. \end{array}} \tag{50}$$

3.4 Global Spatio-temporal Convergence Analysis in 1-D

As in the pointwise case, the analysis for simultaneous global spatio-temporal convergence is significantly more complicated than the previous cases. The analysis for this case can be derived following the procedure for the corresponding pointwise case, given in §2.3.

4 Pointwise Convergence Analysis in n-D

The analysis presented in §2 extends naturally to higher spatial dimensions. For such higher dimensional cases, we consider a variable ξ computed on a given *uniform, logically rectangular* grid, with zoning Δx_i, Δy_j, ..., and *uniform* timestep Δt_l. An example of this case is a 3-D Eulerian hydrocode on a uniform mesh. The fundamental *Ansatz* of pointwise convergence analysis is again that the difference between the exact and computed solutions can be expanded as a function of the spatial and temporal zone sizes:

$$\begin{aligned} \xi^* - \xi^l_{ij\ldots} = \mathcal{A}_1 \, (\Delta x_i)^{p_1} + \mathcal{A}_2 \, (\Delta y_j)^{p_2} + \cdots + \mathcal{B} \, (\Delta t_l)^q \\ + o\Big((\Delta x_i)^{p_1} , (\Delta y_j)^{p_2} , \ldots , (\Delta t_l)^q \Big) \,, \end{aligned} \tag{51}$$

where ξ^* is the *exact* value; $\xi^l_{ij\ldots}$ is the value computed on the grid of spatial zone sizes Δx_i, Δy_j,..., and timestep Δt_l; $\mathcal{A}_1$, $\mathcal{A}_2$,... are the *spatial convergence coefficients*; p_1, p_2,... are the *spatial convergence rates*; $\mathcal{B}$ is the *temporal convergence coefficient*; and q is the *temporal convergence rate*. Consistent with the preceding exposition, this assumption presupposes that the constant error term is absent and that the mixed spatio-temporal terms are negligibly small.

4.1 Pointwise Spatial Convergence Analysis in n-D

We here restrict the above *Ansatz* to spatial convergence only under the assumption that the spatial error is much greater than the temporal error. Suppressing the temporal index l, the following *Ansatz* obtains:

$$\begin{aligned} \xi^* - \xi^l_{ij\ldots} = \mathcal{A}_1 \, (\Delta x_i)^{p_1} + \mathcal{A}_2 \, (\Delta y_j)^{p_2} + \cdots \\ + o\Big((\Delta x_i)^{p_1} , (\Delta y_j)^{p_2} , \ldots , \Big) \,. \end{aligned} \tag{52}$$

4.1.1 Uniform Variables, Differencing, and Zoning

In the case that (1) the independent variables represent fundamentally identical quantities, (2) the differencing in each of these variables is identical, *and* (3) the calculations are conducted on a spatially uniform grid (i.e., $\Delta x_i = \Delta y_j = \cdots$), *significant* simplification occurs. For example, in the case of an algorithm for discretized equations formulated on a 3-D Cartesian grid, (1) each of the coordinate directions has the same units, (2) the equations are typically differenced in an identical fashion in each independent spatial variable, and (3) calculations can be run on a spatially uniform grid. Under these assumptions, the difference between the exact and computed solutions depends only on the grid spacing, which is identical in each direction. The above expansion can be compressed into the *Ansatz* of Eq. 3, viz.,

$$\xi^* - \xi_i^l = \mathcal{A}\ (\Delta x_i)^p + o\Big((\Delta x_i)^p\ ,\Big)\ . \tag{53}$$

The analysis presented in §2.1 applies in this case.

4.1.2 Non-uniform Variables, Differencing, or Zoning

In the case that (1) the independent variables represent fundamentally different quantities, *or* (2) the differencing in each of these variables varies, *or* (3) the calculations are conducted on a spatially non-uniform grid (e.g., $\Delta x_i \neq \Delta y_j$), then *the above simplification cannot be assumed.* For example, in the case of 3-D spherical coordinates, although the differencing in each independent variable may be virtually identical, the zoning almost always differs in the various coordinates, i.e., $\Delta r \neq \Delta\theta \neq \Delta\varphi$. Properly, therefore, a full analysis using all independent variables must be performed.

To illustrate this situation, we consider the case of two independent variables, x and y. The *Ansatz* of Eq. 52 assumes the following form:

$$\xi^* - \xi_{ij}^l = \mathcal{A}_1\ (\Delta x_i)^{p_1} + \mathcal{A}_2\ (\Delta y_j)^{p_2} + o\Big((\Delta x_i)^{p_1}\ , (\Delta y_j)^{p_2}\Big)\ . \tag{54}$$

Two separate analyses result, depending upon whether an exact solution is or is not available.

4.1.3 Example: 2-D Non-uniform Case, Exact Solution Known

In this case, Eq. 54 contains four unknown quantities: $\mathcal{A}_1$, p_1, $\mathcal{A}_2$, and p_2. The following derivation is analogous to that given in §2.3.1 for spatio-temporal convergence. A nonsingular system of four results, each satisfying Eq. 54, is obtained by using solutions computed with the following pairs of spatial zoning: $\{\Delta x, \Delta y\}$, $\{\Delta x/\sigma_1, \Delta y\}$, $\{\Delta x, \Delta y/\sigma_2\}$, and $\{\Delta x/\sigma_1, \Delta y/\sigma_2\}$. From the Eq. 54,

these solutions satisfy the following equalities:

$$\begin{array}{rrrrr} \xi^* - \xi_1 = & \mathcal{A}_1\,(\Delta x)^{p_1} + & & \mathcal{A}_2\,(\Delta y)^{p_2} + \cdots, \\ \xi^* - \xi_2 = & \mathcal{A}_1\,(\Delta x/\sigma_1)^{p_1} + & & \mathcal{A}_2\,(\Delta y)^{p_2} + \cdots, \\ \xi^* - \xi_3 = & \mathcal{A}_1\,(\Delta x)^{p_1} + & \mathcal{A}_2\,(\Delta y/\sigma_2)^{p_2} + \cdots, \\ \xi^* - \xi_4 = & \mathcal{A}_1\,(\Delta x/\sigma_1)^{p_1} + & \mathcal{A}_2\,(\Delta y/\sigma_2)^{p_2} + \cdots. \end{array} \tag{55}$$

These equations form the system of four equations in the four unknown $\mathcal{A}_1$, p_1, $\mathcal{A}_2$, and p_2. The subsequent algebra can be simplified somewhat by considering the following linear combinations of the first and second, and first and third of these equations:

$$\xi_2 - \xi_1 = \left(1 - \sigma_1^{-p_1}\right)\,\mathcal{A}_1\,(\Delta x)^{p_1} + \cdots \tag{56}$$

$$\xi_3 - \xi_1 = \left(1 - \sigma_2^{-p_2}\right)\,\mathcal{A}_2\,(\Delta y)^{p_2} + \cdots. \tag{57}$$

We consider the system of four equations given by the first and last equations in Eq. 55 together with the above two equations. These relations are considered to depend on the variable $\mathbf{a} \equiv [a_1, a_2, a_3, a_4]^T \equiv [\mathcal{A}_1, p_1, \mathcal{A}_2, p_2]^T$:

$$\begin{array}{rrrrr} f_1(\mathbf{a}) = & a_1\,(\Delta x)^{a_2} + & & a_3\,(\Delta y)^{a_4} - (\xi^* - \xi_1) = 0\,, \\ f_2(\mathbf{a}) = & \sigma_1^{-a_2}\,a_1\,(\Delta x)^{a_2} + & & \sigma_2^{-a_4}\,a_3\,(\Delta y)^{a_4} - (\xi^* - \xi_4) = 0\,, \\ f_3(\mathbf{a}) = & \left(1 - \sigma_1^{-a_2}\right)\,a_1\,(\Delta x)^{a_2} & & - (\xi_2 - \xi_1) = 0\,, \\ f_4(\mathbf{a}) = & & \left(1 - \sigma_2^{-a_4}\right)\,a_3\,(\Delta t)^{a_4} - (\xi_3 - \xi_1) = 0\,. \end{array} \tag{58}$$

The typical method of solution of the set of nonlinear equations $\mathbf{f}(\mathbf{a}) = \mathbf{0}$ is Newton's method or some variant thereof. The basic Newton iteration scheme is given in Eq. 26. The required Jacobian $\partial\mathbf{f}/\partial\mathbf{a}$, the inverse of which is typically evaluated numerically, is given below for the above set of equations:

$$\begin{pmatrix} (\Delta x)^{a_2} & a_1\,(\Delta x)^{a_2}\log\Delta x & (\Delta y)^{a_4} & a_3\,(\Delta y)^{a_4}\log\Delta y \\ \sigma_1^{-a_2}\,(\Delta x)^{a_2} & a_1\sigma_1^{-a_2}\,(\Delta x)^{a_2} \times [\log\Delta x - \log\sigma_1] & \sigma_2^{-a_4}\,(\Delta y)^{a_4} & a_3\sigma_2^{-a_4}\,(\Delta y)^{a_4} \times [\log\Delta y - \log\sigma_2] \\ \left(1 - \sigma_1^{-a_2}\right)(\Delta x)^{a_2} & a_1(\Delta x)^{a_2}\left[\sigma_1^{-a_2}\log\sigma_1 + \left(1 - \sigma_1^{-a_2}\right)\log\Delta x\right] & 0 & 0 \\ 0 & 0 & \left(1 - \sigma_2^{-a_4}\right)(\Delta y)^{a_4} & a_3(\Delta y)^{a_4}\left[\sigma_2^{-a_4}\log\sigma_2 + \left(1 - \sigma_2^{-a_4}\right)\log\Delta y\right] \end{pmatrix}. \tag{59}$$

One difficulty involved in solving Eq. 58 is assigning an initial guess that is within the domain of convergence of the iteration. An additional issue is the possibility of obtaining multiple (i.e., nonunique) solutions to this set of nonlinear equations.

These issues, which must be dealt with on a case-by-case basis, illustrate the complications inherent to this approach. In particular, these aspects have conspired to preclude the writing of software sufficiently general to automatically

perform this analysis, which, consequently, is rarely pursued in practice. As suggested by this complexity, we are unaware of any published results along these lines. Nonetheless, analysis of this nature would be required to rigorously demonstrate convergence in the case of non-uniform variables, differencing, or zoning.

4.1.4 Example: 2-D Non-uniform Case, No Exact Solution

In this case, Eq. 54 contains five unknown quantities: $\mathcal{A}_1$, p_1, $\mathcal{A}_2$, p_2, and the exact solution ξ^*. The following derivation is analogous to that given in §2.3.2 for the 1-D spatio-temporal case. A nonsingular system of five results, each satisfying Eq. 54, may obtained by using solutions computed with the following pairs of spatial zoning: $\{\Delta x, \Delta y\}$, $\{\Delta x/\sigma_1, \Delta y\}$, $\{\Delta x, \Delta y/\sigma_2\}$, $\{\Delta x/\sigma_1, \Delta y/\sigma_2\}$, and $\{\Delta x/\sigma_1^2, \Delta y\}$. From the Eq. 54, these solutions satisfy the following equalities:

$$\begin{aligned}
\xi^* - \xi_1 &= \mathcal{A}_1\,(\Delta x)^{p_1} + \mathcal{A}_2\,(\Delta y)^{p_2} + \cdots, \\
\xi^* - \xi_2 &= \mathcal{A}_1\,(\Delta x/\sigma_1)^{p_1} + \mathcal{A}_2\,(\Delta y)^{p_2} + \cdots, \\
\xi^* - \xi_3 &= \mathcal{A}_1\,(\Delta x)^{p_1} + \mathcal{A}_2\,(\Delta y/\sigma_2)^{p_2} + \cdots, \\
\xi^* - \xi_4 &= \mathcal{A}_1\,(\Delta x/\sigma_1)^{p_1} + \mathcal{A}_2\,(\Delta y/\sigma_2)^{p_2} + \cdots. \\
\xi^* - \xi_5 &= \mathcal{A}_1\,\left(\Delta x/\sigma_1^2\right)^{p_1} + \mathcal{A}_2\,(\Delta y)^{p_2} + \cdots,
\end{aligned} \tag{60}$$

These equations form the system of five equations in the five unknown $\mathcal{A}_1$, p_1, $\mathcal{A}_2$, p_2, and ξ^*. The subsequent algebra can be simplified somewhat by considering the following linear combinations of the first and second, first and third, and first and fifth of these equations:

$$\xi_2 - \xi_1 = \left(1 - \sigma_1^{-p_1}\right)\,\mathcal{A}_1\,(\Delta x)^{p_1} + \cdots \tag{61}$$

$$\xi_3 - \xi_1 = \left(1 - \sigma_2^{-p_2}\right)\,\mathcal{A}_2\,(\Delta y)^{p_2} + \cdots \tag{62}$$

$$\xi_5 - \xi_1 = \left(1 - \sigma_1^{-2p_1}\right)\,\mathcal{A}_1\,(\Delta x)^{p_1} + \cdots\,. \tag{63}$$

Consider the system of five equations given by the first and last equations in Eq. 60 together with the above three equations. These relations are considered to depend on the variable $\mathbf{a} \equiv [a_1, a_2, a_3, a_4, a_5]^{\mathrm{T}} \equiv [\mathcal{A}_1, p_1, \mathcal{A}_2, p_2, \xi^*]^{\mathrm{T}}$:

$$\begin{aligned}
f_1(\mathbf{a}) &= a_1\,(\Delta x)^{a_2} + a_3\,(\Delta y)^{a_4} - (a_5 - \xi_1) = 0\,, \\
f_2(\mathbf{a}) &= \sigma_1^{-a_2}\,a_1\,(\Delta x)^{a_2} + \sigma_2^{-a_4}\,a_3\,(\Delta y)^{a_4} - (a_5 - \xi_4) = 0\,, \\
f_3(\mathbf{a}) &= \left(1 - \sigma_1^{-a_2}\right)\,a_1\,(\Delta x)^{a_2} - (\xi_2 - \xi_1) = 0\,, \\
f_4(\mathbf{a}) &= \left(1 - \sigma_2^{-a_4}\right)\,a_3\,(\Delta t)^{a_4} - (\xi_3 - \xi_1) = 0\,. \\
f_5(\mathbf{a}) &= \left(1 - \sigma_1^{-2a_2}\right)\,a_1\,(\Delta x)^{a_2} - (\xi_5 - \xi_1) = 0\,,
\end{aligned} \tag{64}$$

As mentioned in the previous section, Newton's method can be used to solve this nonlinear set of equations. The Jacobian of this set of equations is more complex than in the previous case; due to the algebraic complications, further details are omitted. This derivation illustrates the even greater complexity of

this case and provides the basis by which to implement this analysis, for which, as in the previous subsection, we know of no published results.

4.1.5 Comment: Identical Space-time Locations and Timesteps

The caveats and assumptions raised in §§2.1.4, 2.1.5, and 3.2.3 hold as well in the multidimensional case. Specifically, the computed data being analyzed must be at locations and times identical to (approximately) machine precision; otherwise, the convergence analysis can produce meaningless results. Refer to those sections for a more complete discussion.

4.2 Pointwise Temporal Convergence Analysis in n-D

The analysis provided in section 2.2 for pointwise 1-D temporal convergence properties translates directly into temporal convergence characteristics in the n-dimensional case. Recall that the results of that analysis are based on the assumption that the spatial error dominates temporal error. In the n-D case, one must account for the higher dimensional spatial errors in the term $\mathcal{E}_x$ in Eq. 19. Once this difference is accounted for, however, the resulting expressions for the convergence parameters in Eqs. 20 and 21 remain identical.

4.3 Pointwise Spatio-temporal Convergence Analysis in n-D

Adding temporal dependence further complicates the analysis for n-dimensional convergence. Adding temporal variability to the examples given in §4.1 increases both the algebraic dimensionality and associated solution complexity.

In the case of uniform variables, differencing, and zoning (§4.1.1), the analysis reduces to that of the 1-D spatio-temporal analysis, discussed in §2.3; recall that this case does not have a closed-form solution. For non-uniform variables, differencing, or zoning, the analysis of §4.1.2 is further complicated yet. For example, the analyses discussed in §§4.1.3 and 4.1.4 are increased by one dimension, leading to larger sets of simultaneous nonlinear equations, which do not have closed-form solutions. One can derive the relevant equations, which we do not present, by following the procedures given in those sections.

5 Global Convergence Analysis in n-D

In analogy with the 1-D analysis of §3, we now make the global convergence analysis *Ansatz* that the *norm* of the difference between the exact and computed solutions can be expanded as a function of the spatial and temporal zone sizes:

$$||\xi^* - \xi^l_{ij\ldots}|| = \mathcal{A}_1 \ (\Delta x_i)^{p_1} \ + \ \mathcal{A}_2 \ (\Delta y_j)^{p_2} + \cdots + \mathcal{B} \ (\Delta t_l)^q$$

$$+ \; o\Big((\Delta x_i)^{p_1}, (\Delta y_j)^{p_2}, \ldots, (\Delta t_l)^{q} \Big) , \qquad (65)$$

where, again, ξ^* is the *exact* value; $\xi^l_{ij\ldots}$ is the value computed on the grid of spatial zone sizes Δx_i, Δy_j,..., and timestep Δt_l; $\mathcal{A}_1$, $\mathcal{A}_2$,... are the *spatial convergence coefficients*; p_1, p_2,... are the *spatial convergence rates*; $\mathcal{B}$ is the *temporal convergence coefficient*; and q is the *temporal convergence rate*. We again neglect the constant and mixed error terms in this assumption regarding the form of the error.

5.1 Definition of Norms in n-D

The definitions given in section 3.1 extend naturally to higher dimensions. Specifically, the definition for the L_p functional norm of the function f defined on the set $\Omega \in \mathbb{R}^n$ is

$$||f||_p \equiv \left[\int_\Omega d^n\mathbf{x} \, |f(\mathbf{x})|^p \right]^{1/p} , \qquad (66)$$

where the differential notation $d^n\mathbf{x}$ is used to indicate that the argument $\mathbf{x}$ is an n-vector, i.e., $\mathbf{x} \in \mathbb{R}^n$. Based on this definition, the L_1, L_2, and L_∞ norms are defined as

$$||f||_1 \equiv \int_\Omega d^n\mathbf{x} \, |f(\mathbf{x})| , \qquad (67)$$

$$||f||_2 \equiv \sqrt{\int_\Omega d^n\mathbf{x} \, |f(\mathbf{x})|^2} , \quad \text{and} \qquad (68)$$

$$||f||_\infty \equiv \max_{\mathbf{x}\in\Omega} |f(\mathbf{x})| . \qquad (69)$$

Note that the L_∞ norm is independent of any integral.

We illustrate the multidimensional case by considering the case $n = 2$. In this case, $\Omega = \{ (x, y) \,|\, (x, y) \in [a, b] \times [c, d] \}$. Assume that there are N_x points x_i, $i = 1, \ldots, N_x$, in $[a, b]$, and that there are N_y points y_j, $j = 1, \ldots, N_y$, in $[c, d]$. Let each of these points be the center of a zone of area $\Delta x_i \Delta y_j$. Then, the simplest quadrature scheme is to approximate the the 2D integral as follows:

$$\int_\Omega d^2\mathbf{x} \, g(\mathbf{x}) = \int_a^b dx \int_c^d dy \, g(x, y) \doteq \sum_{i=1}^{N_x} \sum_{j=1}^{N_y} g(x_i, y_j) \, \Delta x_i \, \Delta y_j . \qquad (70)$$

With this assumption, the L_1 and L_2 norms become:

$$||f||_1 \equiv \sum_{i=1}^{N_x} \sum_{i=1}^{N_y} |f(x_i, y_j)| \, \Delta x_i \, \Delta y_j , \qquad (71)$$

$$||f||_2 \equiv \sqrt{\sum_{i=1}^{N_x} \sum_{i=1}^{N_y} |f(x_i, y_j)|^2 \, \Delta x_i \, \Delta y_j} . \qquad (72)$$

For uniform zoning, $\Delta x_i \equiv \Delta x = (b-a)/N_x$ and $\Delta y_j = \Delta y = (d-c)/N_y$, and the above approximations simplify further:

$$||f||_1 \equiv \Delta x\, \Delta y \sum_{i=1}^{N_x} \sum_{j=1}^{N_y} |f(x_i, y_j)| \,, \tag{73}$$

$$||f||_2 \equiv \sqrt{\Delta x\, \Delta y \sum_{i=1}^{N_x} \sum_{j=1}^{N_y} |f(x_i, y_j)|^2} \,. \tag{74}$$

These cases have obvious generalizations to n-dimensional functions.

5.2 Global Spatial Convergence Analysis in n-D

Assuming the spatial error is dominant, we restrict the global *Ansatz* to spatial convergence only, suppress the temporal index l, and obtain

$$\begin{aligned} ||\xi^* - \xi_{ij\ldots}|| = \mathcal{A}_1\ (\Delta x_i)^{p_1} &+ \mathcal{A}_2\ (\Delta y_j)^{p_2} + \cdots \\ &+ o\Big((\Delta x_i)^{p_1}, (\Delta y_j)^{p_2}, \ldots,\Big) \,. \end{aligned} \tag{75}$$

As in the pointwise global spatial analysis in n-D as described in §4.1, the subsequent analysis varies as to whether (1) there are uniform variables, differencing, and zoning, or (2) at least one of these criteria is not met.

5.2.1 Uniform Variables, Differencing, and Zoning

In the former case, the spatial multi-dimensional case reduces to the 1-D case, the analysis of which is given in §3.2. In this case, the analysis is based on the assumption that the above *Ansatz* reduces to

$$||\xi^* - \xi|| = \mathcal{A}\ (\Delta x)^p + o\Big((\Delta x)^p\Big) \,, \tag{76}$$

where we assume that $\Delta x_i = \Delta y_j = \cdots \equiv \Delta x$. By virtue of the assumed differencing and zoning, the dependence of the full error *Ansatz* of Eq. 75 contracts down onto the single independent spatial variable. For the case of a known exact solution, there is an asymptotically valid expression for both the convergence rate p and the convergence coefficient $\mathcal{A}$; if the exact solution is not known, one approximates the exact solution with a solution computed on a fine grid to obtain an estimate of the convergence parameters.

5.2.2 Non-uniform Variables, Differencing, or Zoning

In the case of non-uniformity in the variables, differencing, or zoning, the above simplifications do not obtain, and a full, multi-variate analysis, as described in §§4.1.2, 4.1.3, and 4.1.4, must be undertaken. A complicated analysis obtains

in this case, independent of whether or not an exact solution is available; if not, then a finely zoned computed solution is used as the fiducial "exact" solution and *calculation verification* analysis can be performed.

5.3 Global Temporal Convergence Analysis in n-D

As for the pointwise temporal convergence analysis in n-D discussed in §4.2, the case of global temporal convergence in n-D reduces to the 1-D temporal case, since there is no spatial variations in the computed solutions. The global analogue of the pointwise procedure outlined in §4.2 can be carried out following the 1-D global spatial convergence analysis given in §3.2. That analysis, based on different spatial grid sizes in 1-D, translates directly into the present case by exchanging spatial and temporal dependences, so that one uses normed values evaluated with different (uniform) timesteps and identical spatial grids in all simulations.

5.4 Global Spatio-temporal Convergence Analysis n-D

As in the pointwise n-D case, the analysis for simultaneous global spatio-temporal convergence is significantly more complicated than the previous cases. The details of this case follows naturally from the analysis given in §2.3, with suitable generalization.

6 Convergence Analysis with Arbitrarily Structured Data

Convergence analysis of non-uniformly structured data, such as might be obtained from Lagrangian [4], alternating Lagrangian-Eulerian (ALE) [13], or adaptive mesh refinement (AMR) [15] hydrodynamics code, presents a significantly knottier problem than the uniformly structured data heretofore considered. In this section, we discuss some options for performing such an analysis.

The most straightforward manner by which to perform this analysis is to interpolate the non-uniformly structured data onto a uniformly zoned mesh. That is, one transforms the data to a form that is consistent with the convergence analysis algorithm that has been developed. This approach introduces the issue of remeshing data, which, while relatively straightforward for smooth data, is significantly more perilous for discontinuous data (for which conservative rezoning strategies may be appropriate [14]). We suspect—although we offer no explicit proof—that, if the remeshing is of order greater than or equal to that of the convergence, then this procedure should produce valid convergence results.

Alternatives to this approach follow from revisiting the fundamental notions underpinning convergence analysis. Recall that the entire convergence analysis procedure is based upon the *Ansatz* that the error in the computed solution

varies as some power of the discretized grid size (see, e.g., Eq. 1). This equation codifies the intuitively appealing assumption, made *a priori*, that the discrepancy between the exact and computed solution is related to the resolution of the computed solution in some prescribed, *direct* manner. This assumption follows, of course, from the fundamental numerical analysis of the solution algorithms for the underlying equations (ODEs and PDEs). This notion can be generalized to the concept that the solution error is related to the *resources* used to obtain that solution in a prescribed, *inverse* manner. That is, a convergent situation is characterized as one for which the greater the resources applied to the solution, the smaller the solution error. We expand upon these ideas in the following subsections, restricting our consideration to the canonical case of spatial convergence analysis in 1-D; these notions can be naturally extended to temporal convergence and higher spatial dimensions.

6.1 1-D Convergence Analysis of Arbitrarily Data Assuming Direct Dependence

For the case of 1-D unstructured data (with Lagrangian, ALE, or AMR grids being the tacit archetypes), in which any temporal dependence is neglected, we again assume spatial error dominates and make the *Ansatz* that

$$\xi^* - \xi_i = \mathcal{A}\ (\Delta\tilde{x})^p + o\Big((\Delta\tilde{x})^p\Big)\,, \tag{77}$$

where, as before, ξ^* is the exact value, ξ_i is the value computed on the grid with *characteristic* spatial zone size $\Delta\tilde{x}$, $\mathcal{A}$ is the spatial convergence coefficient, and p is the spatial convergence rate. Here we explicitly assume that the inaccuracy of the solution depends *only* on the characteristic scale used in the calculation, $\Delta\tilde{x}$. There are many different ways this characteristic value may be defined; in the following, we suggest the two most obvious. This quantity may be defined as the *mean* zone size:

$$\Delta\tilde{x} = \frac{1}{N_x} \sum_i\ \Delta x_i\,, \tag{78}$$

where N_x is the total number of zones in the mesh; this value has obvious higher-dimensional analogues. Alternatively, $\Delta\tilde{x}$ may be defined as the *minimum* zone size:

$$\Delta\tilde{x} = \min_i\ \Delta x_i\,, \tag{79}$$

The minimum mesh spacing in 1-D generalizes naturally to higher dimensions: for AMR meshes, the corresponding quantity is obvious, while for more general (e.g., Lagrangian) meshes, this quantity could be taken, e.g., in 2-D as the square root of the zone with minimum area and in 3-D as the cube-root of the zone with minimum volume.

For the solution on a coarse grid, denoted with the subscript c, $\Delta\tilde{x}_c \equiv \Delta\tilde{x}$, and Eq. 3 implies

$$\xi^* - \xi_c = \mathcal{A}\ (\Delta\tilde{x})^p + \cdots \tag{80}$$

The machinery developed in the previous sections then applies. We omit the details and provide the following formulas for (generalized) convergence metrics, viz., the convergence rate p and convergence coefficient $\mathcal{A}$.

In the case of an available exact solution ξ^*, the pointwise estimators of convergence are:

$$\boxed{\begin{array}{rcl} p & \equiv & \left[\log\left[\xi^* - \xi_c\right] - \log\left[\xi^* - \xi_m\right]\right] \Big/ \log\tilde{\sigma}\,, \\ \mathcal{A} & \equiv & \left[\xi^* - \xi_c\right] \,/\, (\Delta\tilde{x})^p\,. \end{array}} \tag{81}$$

The corresponding global convergence metrics are:

$$\boxed{\begin{array}{rcl} p & \equiv & \left[\log||\xi^* - \xi_c|| - \log||\xi^* - \xi_m||\right] \Big/ \log\tilde{\sigma}\,, \\ \mathcal{A} & \equiv & ||\xi^* - \xi_c|| \,/\, (\Delta\tilde{x})^p\,. \end{array}} \tag{82}$$

In the above expressions, $\tilde{\sigma}$ is the ratio of the characteristic zone sizes, i.e., $\tilde{\sigma} = \Delta\tilde{x}_c/\Delta\tilde{x}_m$. When no exact solution is available, the fundamental *Ansatz* is modified, resulting in replacement of the exact solution ξ^* in Eqs. 81 and 82 with a fine-grid solution ξ_f.

The convergence metrics obtained from Eqs. 81 and 82 may differ from those obtained from the uniform-grid case, even for identical problems. The error *Ansatz* of Eq. 3 is a relation based on a uniform cell size, Δx. In contrast, the convergence properties assumed in Eq. 77 are related to the solution algorithm behavior on the scale of some characteristic zone size, $\Delta\tilde{x}$. The convergence metrics obtained from these two assumptions may be quite different for simulations of the identical problem computed on uniform and non-uniform grids. We know of no mathematical foundation for making a comparison between uniform and non-uniform convergence metrics; nevertheless, these two verification analyses should provide identical convergence metrics in the limit as the two zone sizes approach a uniform value.

Using the mean or minimum zone size represent only two of many possible characterizations for the convergence behavior. In addition to using either of these length scales for arbitrarily structured grids, an additional characteristic scale is obtained by multiplying the mean length scale by the ratio of the minimum to maximum grid spacings:

$$\Delta\tilde{x} = \Delta x_{\text{mean}} \times \left(\Delta x_{\text{min}}/\Delta x_{\text{max}}\right)\,. \tag{83}$$

The convergence metrics obtained from this *Ansatz* may differ from others, even for the same problem. Further investigation for optimally representative error *Ansätze* (which may be problem-dependent) and the relationship between the corresponding convergence metrics is warranted.

6.2 1-D Convergence Analysis of Arbitrarily Data Assuming Indirect Dependence

An alternative viewpoint is to assume that the solution error varies inversely as the amount of resources used in the calculation. Intuitively, convergent behavior is characterized by a more accurate solution on a finely zoned calculation than on a coarsely zoned calculation, i.e., from a calculation that uses more resources. For the case of 1-D unstructured data in which temporal dependence is neglected, this approach suggests the *Ansatz* that

$$\xi^* - \xi_i = \mathcal{A}\ (1/N)^p + o\Big((1/N)^n\Big)\,, \tag{84}$$

where N is the *total number of zones* used in the calculation. This assumption bears similarity to the approach used in the finite element community, in which the the solution error is assumed to vary inversely with the degrees of freedom of the solution method (so that a convergent solution with more degrees of freedom implies smaller error). The previous analysis may be applied in this case, too, resulting in the following convergence metrics:

$$\boxed{\begin{array}{rcl} p & \equiv & \big[\log\left[\xi^* - \xi_c\right] - \log\left[\xi^* - \xi_m\right]\big] \big/ \log\tilde{\sigma}\,, \\ \mathcal{A} & \equiv & \left[\xi^* - \xi_c\right]\ N_c^n\,. \end{array}} \tag{85}$$

The corresponding global convergence metrics are:

$$\boxed{\begin{array}{rcl} p & \equiv & \big[\log||\xi^* - \xi_c|| - \log||\xi^* - \xi_m||\big] \big/ \log\tilde{\sigma}\,, \\ \mathcal{A} & \equiv & ||\xi^* - \xi_c||\, N_c^p\,. \end{array}} \tag{86}$$

In these expressions, $\tilde{\sigma}$ is the ratio of the number of zones in the medium mesh to the number in the coarse mesh, i.e., $\tilde{\sigma} = N_m/N_c > 1$. As in the previous case, when no exact solution is available, the fundamental *Ansatz* is modified, resulting in replacement of ξ^* in Eqs. 85 and 86 with ξ_f.

As in the previous section, the error *Ansatz* of Eq. 84 represents only one possible description of convergence behavior. The convergence metrics obtained using this assumption may differ from the uniform-grid case, even for identical problems. Convergence metrics obtained from Eqs. 85 or 86 should approach the corresponding values for the uniform-grid case as the zone sizes approach a uniform value. Further investigation of the various error *Ansätze* and the relationship among convergence metrics is warranted.

7 Examples

In this section, we present examples of the foregoing analysis. Specifically, in §7.1 we present analysis of a 1-D uniform grid coupled physics problem, in §7.2 we analyze a 1-D nonuniform grid single physics problem, and in §7.3 we present verification results for a 3-D uniform grid single physics problem.

7.1 1-D Uniform Grid Case

In this section, we demonstrate the verification metrics described above for the case of a 1-D problem coupling hydrodynamics coupled with radiation-conduction on a uniform grid, using an Eulerian formation of the underlying equations. The problem considered is that originally published by Reinicke and Meyer-ter-Vehn (RMtV)[18]. We provide a brief description of the problem and analysis and refer to [9] for more information regarding this problem, its solution, and convergence analysis of it.

The set of evolution equations governing this problem is given in physical space as

$$\rho_t + u\,\rho_r + \frac{\rho}{r^{n-1}}\,\left(r^{n-1}\,u\right)_r = 0\,, \tag{87}$$

$$u_t + u\,u_r + \frac{1}{\rho}\,p_r \qquad\qquad = 0\,, \tag{88}$$

$$e_t + u\,e_r - \frac{p}{\rho^2}\,\left(\rho_t + u\,\rho_r\right) \;= -\frac{1}{\rho\,r^{n-1}}\,\left(r^{n-1}\,S\right)_r\,, \tag{89}$$

where r is the spatial variable, ρ is the density, u is the velocity, p is the pressure, e is the specific internal energy, $S \equiv -\chi\,T_r$ is the heat flux with conductivity χ, and T is the temperature. The parameter $n = 1$, 2, or 3 is the dimensionality index for one-dimensional planar, cylindrical, or spherical geometry, respectively.

Three additional assumptions are made. First, the polytropic gas equation of state holds, so that

$$(\gamma - 1)\;e = p/\rho = \mathcal{G}\,T\,, \tag{90}$$

where γ is the adiabatic exponent (equal to the ratio of specific heats in this case) and $\mathcal{G}$ is the product of the specific heat at constant volume c_v and the Grüneisen coefficient Γ. Second, the heat conductivity χ has the form

$$\chi = \chi_0\,\rho^a\,T^b \qquad \text{where} \qquad a \le 0 \quad \text{and} \quad b \ge 1\,. \tag{91}$$

Third, the flow is evolving into a cold (i.e., $T = 0$) gas with a power-law initial density profile given by

$$\rho_0(r) \propto r^\kappa\,, \tag{92}$$

where κ is a negative real number.

We consider solutions to these equations for the case of a spherically symmetric, blast-wave-like problem with an initial delta-function energy source that is located at the origin. The initial energy is assumed to be of sufficient magnitude so that conduction dominates hydrodynamics, i.e., so that the thermal front leads the hydrodynamic shock. As shown by RMtV, the solution of the PDEs in Eqs. 87–89 reduces to the solution to a set of coupled nonlinear ODES; see [18] for details. The solution to this problem contains two discontinuities:

at the heat front and at the hydrodynamics shock. These discontinuities make obtaining an accurate solution to the reduced ODEs a challenge; this hurdle, however, can be overcome, as discussed in [9]. That reference contains a description of the procedure by which a solution of the reduced ODEs is related to a hydrocode solution to the full PDEs; this correspondence procedure, while straightforward, requires careful attention to solution details.

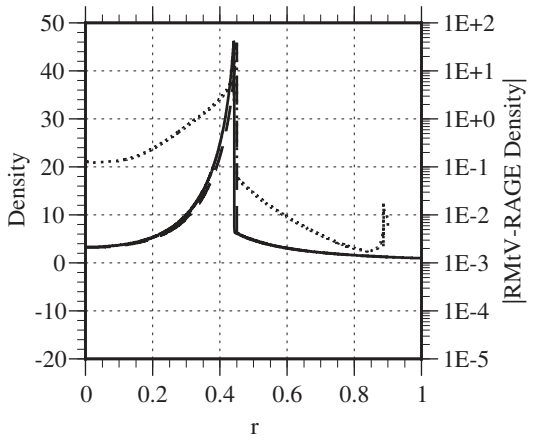

Figure 2: Density results for the RMtV problem described in [9, 18]. The solid lines are the Crestone project code results with 3200 points on $[0, 1]$; the dashed lines are the RMtV reduced-ODE results at the same locations as the hydrocode results; the dotted lines, plotted against the right axes, are the absolute differences between the solutions.

Figure 2 contains a plot of the "exact" (i.e., ODE-based) and hydrocode solutions for the density as a function of radius at for the RMtV configuration described in [9, 18]. The solid line in this figure shows the Crestone project code results with 3200 equally-spaced zones on the interval $0 \leq r \leq 1$, the dashed line represents the solution to the reduced RMtV ODEs, and the dotted line (plotted against the right ordinate) gives the absolute difference between the two solutions. As shown, the greatest discrepancy is at the hydrodynamic shock (located at $r \doteq 0.45$).

Figure 3 contains a plot of the global L_1 norm of the difference between the "exact" (i.e., ODE-based) and hydrocode solutions for the density of the same RMtV configuration. Since this is a three-dimensional problem that is spherically symmetric, the L_1 norm of the errors is evaluated based on Eq. 67; due to the symmetry, however, these integrals analytically reduce to integration over radius (r) only. The abscissae in this plot are (i) the cell size (bottom) and (ii) the number of cells per unit coordinate interval (top). The convergence

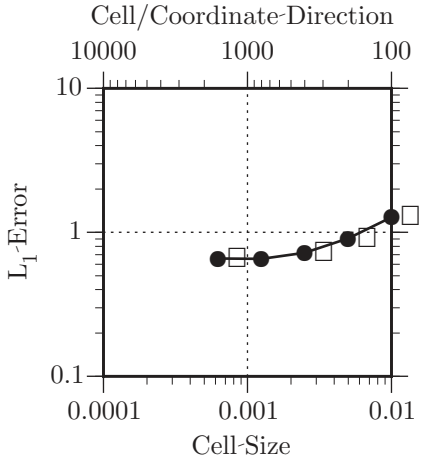

Figure 3: Errors in the density, reckoned with the L_1 norm on a 1-D spherically symmetric mesh, for the RMtV problem results. The solid dots are the L_1 error (see Eq. 67) plotted against the cell size (bottom abscissa) or, equivalently, the number of zones per unit coordinate (top abscissa).

rates corresponding to these errors are given in Table 1, which shows that the positive convergence rates on the coarser grids decreases to effectively zeroth-order at the finger grids. This lack of convergence on the finer zones is related to the non-zero error in shock position evident in Fig. 2. This error remains finite under mesh refinement—hence the zeroth order convergence result suggested in Fig. 3 and quantified in Table 1.

Cell Size	10^{-2}	5×10^{-3}	2.5×10^{-3}	1.25×10^{-3}	6.25×10^{-3}
Cells on $[0, 1]$	100	200	400	800	1600
L_1 Error	1.27	0.908	0.722	0.656	0.658

	$100 \rightarrow 200$	$200 \rightarrow 400$	$400 \rightarrow 800$	$800 \rightarrow 1600$
L_1 Convergence Rate	0.49	0.33	0.14	-4.2×10^{-3}

Table 1: L_1 norm of the density errors at different grid resolutions (top) and associated convergence rates (bottom) for the RMtV problem.

7.2 1-D Non-Uniform Grid Case

In this section, we demonstrate the verification metrics proposed above for the case of a 1-D pure hydrodynamics calculation on a non-uniform grid, using a Lagrangian formation of the underlying hydrocode equations. The numerical method is taken from the compatible Lagrangian method of Caramana et al. [4] using a flux-limited artificial viscosity.

We examine the results on Sod's shock tube problem [23] using four different mesh resolutions: 100, 200, 400 and 800 zones on the unit interval. Sod's shock tube problem is defined by and 8:1 jump in density and a 10:1 jump in pressure in an initially stationary $\gamma = 1.4$ polytropic gas. We take the higher pressure and density equal to unity and compute the solution to a uniform time of $t = 0.2$. The exact solution is available using the techniques described by Gottlieb and Groth [6].

While the calculations are compared at exactly the same temporal location, the Lagrangian mesh does not allow the solution to be compared at identical spatial locations. To overcome this difficulty, the mesh locations of the Lagrangian mesh are used to compute the analytic solution at the identical set of locations. For the L_1 norm, the error must be computed as weighted by the mesh spacing, because that spacing is nonuniform. For example, the L_1 norm is computed according to Eq. 39. These norms are used to infer the convergence rate, which is computed according to Eq. 82, where the *mean* zone size is used. That is, the value of $\Delta\tilde{x}$ in the error *Ansatz* is taken to be the length of the total computational interval divided by the total number of zones.

Table 2 shows the L_1 errors as computed using the actual and simulated densities. These values indicate that the code converges at approximately first-order in this measure. These results are entirely consistent with other shock capturing methods for this problem. The plots in Fig. 4 show the actual solutions for density and the corresponding errors at each resolution. In the density plot, the exact solution is a solid line; in both the density and error plots, finely dashed lines corresponding to the solution with 800 zones on the unit, with increasingly more coarsely dashed lines representing solutions with 400, 200, and 100 zones. The error plot shows that the greatest error is incurred at the shock, with the contact discontinuity and the rarefaction wave (specifically, the head and tail thereof) being the prime additional error sites. Together, these plots demonstrate that error quantification reveals much more information than can be discerned from the plot of the computed solution alone.

This analysis demonstrates that verification of a code against an exact solution on a nonuniform mesh can be a matter of slight complication over the uniform case. On the other hand, conducting self-convergence analysis may considerably more difficult because the data are at differing locations.

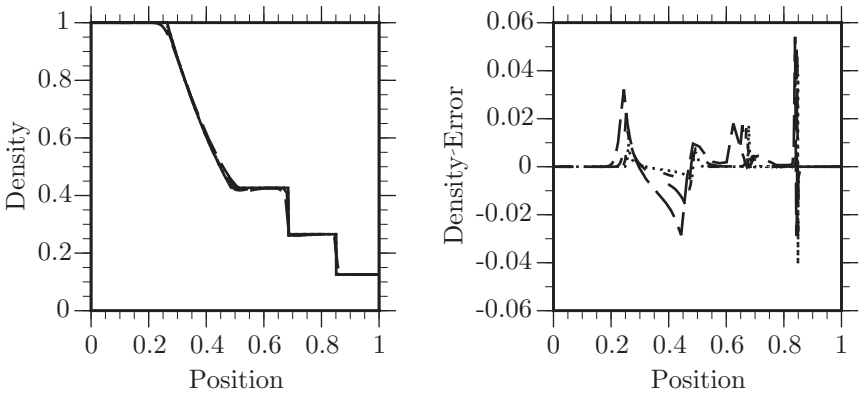

Figure 4: The left image shows the solutions compared with the exact solution, and the right image shows the errors in the same set of calculations.

7.3 3-D Uniform Grid Case

In this section, we demonstrate the verification metrics proposed above for the case of a 3-D pure hydrodynamics calculation on a uniform grid, using an Eulerian formation of the underlying equations. We consider the Sedov problem for a point-blast in a uniform medium [2, 22, 24]. We offer a brief description of the problem and analysis and refer to [10] for more information regarding this problem, its solution, and convergence analysis based on it.

The set of evolution equations governing this problem is given in physical space as

$$\rho_t + u\,\rho_r + \frac{\rho}{r^{j-1}}\,\left(r^{j-1}\,u\right)_r \quad = \quad 0\,, \tag{93}$$

Initial Cell Size	10^{-2}	5×10^{-3}	2.5×10^{-3}	1.25×10^{-3}
Cells on $[0,1]$	100	200	400	800
L_1 Error	5.76×10^{-3}	2.90×10^{-3}	1.47×10^{-3}	7.49×10^{-3}

	$100 \rightarrow 200$	$200 \rightarrow 400$	$400 \rightarrow 800$
L_1 Convergence Rate	0.99	0.98	0.97

Table 2: L_1 norm of the density errors at different grid resolutions (top) and associated convergence rates (bottom) for the Lagrangian Sod problem.

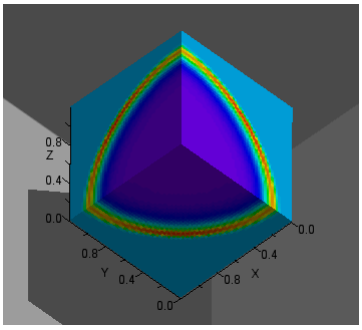

Figure 5: Density field for the Sedov problem described in [10, 22] as computed by the Crestone project code results with 1.728×10^6 cells in $[0, 1.2] \times [0, 1.2] \times [0, 1.2]$.

$$u_t + u\, v_r + \frac{1}{\rho}\, p_r = 0\,, \tag{94}$$

$$(p/\rho^\gamma)_t + u\ (p/\rho^\gamma)_r = 0\,, \tag{95}$$

where ρ is the density, u is the speed, and p is the pressure. The parameter $j = 1$, 2, or 3 is the dimensionality index for one-dimensional planar, cylindrical, or spherical geometry, respectively. In the spherical case we consider, u is magnitude of the radial velocity. Implicit in these evolution equations is the assumption of a polytropic gas equation of state (Eq. 90). The flow is assumed to evolve into an initially zero-pressure, uniform (constant) density gas. The more general case of an initial power-law density is discussed in [22, 10].

We consider solutions to these equations for the case of a spherically symmetric problem with an initial delta-function energy source at the origin. As shown by Sedov [22], the solution of the PDEs in Eqs. 93–95 reduces to explicit expressions involving polynomial and transcendental functions; evaluation of the parameters involved in that solution, however, does require numerical quadrature. A description of the closed-form solution to this problem, together with a pseudo-code algorithm by which to obtain solutions, is given in [10].

Figure 5 contains a plot of the Crestone project code results for this problem run in full 3-D geometry with 120 equally-spaced zones on the domain $\{(x, y, z) \,|\, (x, y, z) \in [0, 1.2] \times [0, 1.2] \times [0, 1.2]\}$. The values near a radius of unity correspond to the shock position. The computed solution is for the 3-D Cartesian-geometry problem; by the symmetry of the initial conditions, the governing equations are identical to the 1-D spherically symmetric form of the PDEs given in Eqs. 93–95. Figure 6 shows a plot of the global L_1 norm of the difference between the "exact" and hydrocode solutions for the density for this problem. Since this is a genuinely three-dimensional problem, the L_1 norm of the errors is calculated according to the full 3-D integral form of Eq. 67. The abscissae in this

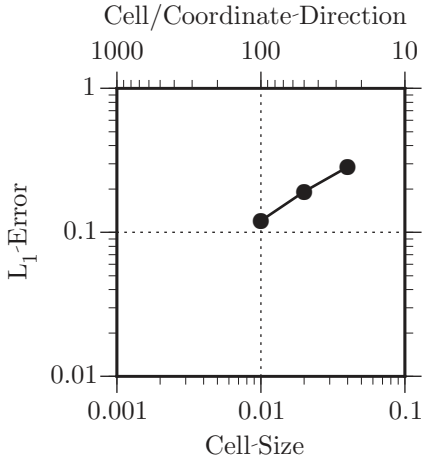

Figure 6: Errors in the density, reckoned with the L_1 norm on the 3-D mesh, for the Sedov problem results. The solid dots are the L_1 error (see Eq. 67) plotted against the cell size (bottom abscissa) or, equivalently, the number of zones per unit coordinate (top abscissa).

plot are (i) the cell size (bottom) and (ii) the number of cells per unit coordinate interval (top). The convergence rates corresponding to these errors are given in Table 3, which shows positive convergence rates across the entire domain considered. This problem indirectly illustrates the challenge of multidimensional verification problems: to perform the 3-D calculations needed for this analysis requires considerable computational resources—and finer grid resolution would require even more.

Cell Size	4×10^{-2}	2×10^{-2}	10^{-2}
Cells on $[0,1]$	25	50	100
Cells on $[0,1] \times [0,1] \times [0,1]$	1.5625×10^4	1.25×10^5	10^6
L_1 Error	0.283	0.192	0.120

	$25 \rightarrow 50$	$50 \rightarrow 100$
L_1 Convergence Rate	0.56	0.68

Table 3: L_1 norm of the density errors at different grid resolutions (top) and associated convergence rates (bottom) for the Sedov problem.

7.4 Pointers to Other Examples

The problems considered in the preceding sections exemplify some aspects of convergence analysis for the numerical solution of PDEs. Additional examples are given in previously cited works [7, 8, 9, 10]. As the following references (and the citations therein) suggest, there are additional examples of convergence studies and verification analysis available in the literature.

No discussion of hydrocode verification is complete without reference to the pioneering work of Roache, compiled in Roache [19]. This book offers a complete introduction to verification analysis. A thorough discussion of convergence analysis, with detailed descriptions of underlying assumptions and their implications, is provided in the comprehensive report of Oberkampf & Trucano [16]. This carefully written and researched work, which we recommend highly, contains an extensive and valuable bibliography of relevant references as well as a useful exposition on the complementary issue of code validation. Further overview material is contained in the document summarizing a recent ASCI/NNSA Verification Workshop [11]. Additional ASC-relevant examples are given in [17]. Salari & Knupp [21] discuss the *method of manufactured solutions* approach, which provides an avenue by which to ascertain convergence properties for smooth problems in the absence of known exact solutions. Many problems of interest, however, contain complex flow discontinuities; as pointed out by Oberkampf & Trucano, such problems violate the foundational assumption of solution smoothness, which affects the subsequent convergence analysis. Theoretical aspects of this topic are addressed by Kimoto & Chernoff [12] and Engquist & Sjögreen [5]. Practical aspects of the effects of shocks on the convergence computed flows and how to quantify the subsequent behavior are examined in the work of Roy [20].

8 Summary

In this note we have shown how to perform convergence analysis for verifying algorithms for PDEs used in hydrocodes. This analysis plays a principal role in code physics verification, which, as a component of verification and validation, is one of the main tenets necessary for establishing credibility of a computer-algorithm-based simulation process. We have derived explicit metrics, viz., the values characterizing the convergence properties of an algorithm implemented to obtain numerical solutions of discretized approximations to PDEs. These metrics provide repeatable gauges that quantify the convergence of the software implementation of the underlying algorithms. The process of evaluating these metrics represents the essence of verification analysis.

The fundamental assumption of this analysis is that the error in the computed solution varies as the computational cell sizes and timestep raised to some power; these exponents are the convergence rates. The analysis provided herein

can, however, also be applied to the analysis of more general algorithms and physics, including but not limited to the convergence characteristics of solution functionals (e.g., shock position). These quantities can be used as well in mesh resolution studies in the absence of exact solutions; such calculation verification is a critical component by which to quantify software behavior for complicated configurations or complex equations (e.g., those of coupled physics).

The results for 1-D spatial convergence analysis are spelled out in detail in §2. The spatial error in PDE solutions typically dominates the temporal error, so characterization of these properties is particularly important. Key results of §2 include: Eq. 6, which gives the pointwise convergence results when the exact solution is known; Eqs. 13 and 14, which give the pointwise convergence results when the exact solution is not known; and Eq. 46, which gives the global convergence rate when the exact solution is known. The approach to convergence analysis of the analogous 1-D cases for temporal and spatio-temporal behavior is also described, as are the higher-dimensional cases. As shown in §4.1.3, the analysis of spatial convergence for the simplest higher-dimensional (viz., 2-D) case leads to a set of complicated nonlinear equations that do not possess a closed-form solution.

In §6 we describe approaches to convergence analysis on irregular, nonuniform meshes, as seen, e.g., in Lagrangian, ALE, or AMR meshes. We discuss three different assumptions by which the solution error can be quantified in these cases. The meaningful quantitative verification analysis of such cases is, however, an open research topic. Our proposed approaches provide verification metrics consistent with those provided elsewhere in this report; however, future research may reveal more suitable gauges of code convergence in such cases. Section 7 contains examples of this analysis method. Results are given for convergence rates for different computer codes on single- and multi-physics problems, and for both 1-D and 3-D simulations.

Using the methodology presented herein, one can implement a consistent convergence analysis procedure by which to verify software implementations of discrete numerical methods for the simulations of continuous phenomena.

Acknowledgements

The authors wish to acknowledge ongoing and enlightening discussions with Michael Clover and Rob Lowrie on code verification issues. This work was performed at Los Alamos National Laboratory, which is operated by the University of California for the United States Department of Energy under contract W-7405-ENG-36.

References

[1] D. J. Benson, Computational Methods in Lagrangian and Eulerian Hydrocodes, *Computer Methods Applied Mechanics Eng.* **99**, pp. 235–394 (1992).

[2] H. A Bethe, K. Fuchs, J. O. Hirschfelder, J. L. Magee, R. E. Peierls, J. von Neumann, *Blast Wave*, Los Alamos Scientific Laboratory Report LA-2000 (1947).

[3] J. Cadafalch, C. C. Pérez-Segarra, R.Cònsul, A. Oliva, Verification of Finite Volume Computations on Steady-State Fluid Flow and Heat Transfer, *J. Fluids Eng.* **124**, pp. 11–21 (2002).

[4] E. J. Caramana, D. E. Burton, M. J. Shashkov, P. P. Whalen, The Construction of Compatible Hydrodynamics Algorithms Utilizing Conservation of Total Energy, *J. Comp. Phys.* **146**, pp. 227–262 (1998).

[5] B. Engquist, B. Sjögreen, The convergence rate of finite difference schemes in the presence of shocks, *SIAM J. Num. Anal.* **35**, pp. 2464–2485 (1998).

[6] J. J. Gottlieb, C. P. T. Groth, Assessment of Riemann Solvers for Unsteady One-Dimensional Inviscid Flows of Perfect Gases, *J. Comp. Phys.* **78**, pp. 437–458 (1988).

[7] J. R. Kamm, W. J. Rider, *2-D Convergence Analysis of the RAGE Hydrocode*, Los Alamos National Laboratory Report LA-UR-98-3872 (1998).

[8] J. R. Kamm, W. J. Rider, *Verification Analysis of the Direct Eulerian 2-D RAGE Hydrodynamics Algorithm*, Los Alamos National Laboratory Report LA-UR-99-5234 (1999).

[9] J. R. Kamm, *Investigation of the Reinicke & Meyer-ter-Vehn Equations: 1. The Strong Conduction Case*, Los Alamos National Laboratory Report LA-UR-00-4304 (2000).

[10] J. R. Kamm, *Evaluation of the Sedov-von Neumann-Taylor Blast Wave Solution*, Los Alamos National Laboratory Report LA-UR-00-6055 (2000).

[11] J. R. Kamm ed., *Summary of the ASCI/NNSA Verification Workshop 2001*, Los Alamos National Laboratory Report LA-UR-02-0313 (2001).

[12] P. A. Kimoto, D. F. Chernoff, Assessment of Riemann Solvers for Unsteady Convergence properties of finite-difference hydrodynamics schemes in the presence of shocks, *App. J. Supp. Ser.* **96**, pp. 627–641 (1995).

[13] L. G. Margolin, Introduction to "An arbitrary Lagrangian-Eulerian computing method for all flow speeds", *J. Comp. Phys.* **135**, pp. 198–202 (1997).

[14] L. G. Margolin & M. Shashkov, *Second-Order Sign-Preserving Remapping on General Grids*, Los Alamos National Laboratory Report LA-UR-02-525 (2002).

[15] G. H. Miller, E. G. Puckett, A high-order Godunov method for multiple condensed phases, *J. Comp. Phys.* **128**, pp. 134–164 (1996).

[16] W. L. Oberkampf, T. G. Trucano, *Verification and Validation in Computational Fluid Dynamics*, Sandia National Laboratories Report SAND2002-0529 (2002).

[17] D. Post et al., *Report of the Activities for the Completion of the V&V Level-1 Milestone for Initial Validation Methodology for Early-Time Primary Behavior by the Los Alamos National Laboratory (U)*, Los Alamos National Laboratory Report LA-CP-01-259 (2001).

[18] R. Reinicke, J. Meyer-ter-Vehn, The point explosion with heat conduction, *Phys. Fluids A* **3**, pp. 1807–1818 (1991).

[19] P. J. Roache, *Verification and Validation in Computational Science and Engineering*, Hermosa Publishers, Albuquerque, NM (1998).

[20] C. J. Roy, Grid convergence error analysis for mixed-order numerical schemes, submitted to *AIAA J.* (2001).

[21] K. Salari, P. Knupp, *Code Verification by the Method of Manufactured Solutions*, Sandia National Laboratories Report SAND2000-1444 (2000).

[22] L. I. Sedov, *Similarity and Dimensional Methods in Mechanics*, Academic Press, New York, NY, p. 147 ff. (1959).

[23] G. Sod, A Survey of Several Finite Difference Methods for Systems of Nonlinear Hyperbolic Conservation Laws, *J. Comp. Phys.* **27**, pp. 1–31 (1978).

[24] G. I. Taylor, The formation of a blast wave by a very intense explosion, *Proc. Roy. Soc. London A* **201**, pp. 159–174 (1950).